

PAPER • OPEN ACCESS

New features of doubly transient chaos: complexity of decay

To cite this article: György Károlyi and Tamás Tél 2021 *J. Phys. Complex.* **2** 035001

View the [article online](#) for updates and enhancements.

OPEN ACCESS

PAPER



New features of doubly transient chaos: complexity of decay

RECEIVED

22 December 2020

REVISED

26 February 2021

ACCEPTED FOR PUBLICATION

11 March 2021

PUBLISHED

15 April 2021

Original content from this work may be used under the terms of the [Creative Commons Attribution 4.0 licence](#).

Any further distribution of this work must maintain attribution to the author(s) and the title of the work, journal citation and DOI.

György Károlyi^{1,*} and Tamás Tél^{2,3} ¹ Institute of Nuclear Techniques, Budapest University of Technology and Economics, Műgyetem rkp. 3, 1111 Budapest, Hungary² Institute for Theoretical Physics, Eötvös University, Pázmány Péter sétány 1/A, H-1117 Budapest, Hungary³ MTA-ELTE Theoretical Physics Research Group, Pázmány Péter sétány 1/A, H-1117 Budapest, Hungary

* Author to whom any correspondence should be addressed.

E-mail: karolyi@reak.bme.hu**Keywords:** transient chaos, doubly transient chaos, autonomous dissipative systems**Abstract**

In dissipative systems without any driving or positive feedback all motion stops ultimately since the initial kinetic energy is dissipated away during time evolution. If chaos is present, it can only be of transient type. Traditional transient chaos is, however, supported by an infinity of unstable orbits. In the lack of these, chaos in undriven dissipative systems is of another type: it is termed doubly transient chaos as the strength of transient chaos is diminishing in time, and ceases asymptotically. Here we show that a clear view of such dynamics is provided by identifying KAM tori or chaotic regions of the dissipation-free case, and following their time evolution in the dissipative dynamics. The tori often smoothly deform first, but later they become disintegrated and dissolve in a kind of shrinking chaos. We identify different dynamical measures for the characterization of this process which illustrate that the strength of chaos is first diminishing, and after a while disappears, the motion enters the phase of ultimate stopping.

1. Introduction

The phenomenon of chaos [1–5] is often illustrated with simple undriven experimental set-ups like magnetic pendulum, double pendulum or bouncing of a ball on a double wedge. They clearly exhibit complex motion, and are generally accepted as faithful demonstrations of chaos. The particular example of magnetic pendulum is widely used also as a paradigmatic example for the fractality of basin boundaries (see e.g. [6]) subsequent magnifications of which would exhibit scale invariance.

A closer inspection, however, reveals that the intensity of such motions decreases in time due to the unavoidable air drag or different kinds of friction. A theoretical consideration opens up a real paradox: the long-time asymptotics of such dynamics is without any motion, the attractor is one fixed point, or perhaps the set of a few. This would allow for traditional transient chaos [4, 7, 8], however, it would also require a steady non-attracting chaotic set, a chaotic saddle as the union of an uncountable infinity of unstable orbits, which does exist in periodically driven systems, but not in purely dissipative systems.

As a consequence, the basin boundaries cannot be true fractals, they do not exhibit scale invariance. The authors of [9–12] formulated that in such cases the properties of the chaotic-like dynamics exhibited outside the attractors changes in time. Hence the underlying chaotic set, a chaotic saddle, is also time-dependent, i.e. the saddle itself is also transient (and ceases to be chaotic ultimately). The term doubly transient chaos was coined and it was claimed that this is the generic form of chaos in autonomous dissipative systems. The associated behavior is thus of a completely different type compared to the one previously established for driven dissipative systems, to traditional transient chaos. These properties were investigated in cases of the magnetic pendulum [9], of the decaying motion of a ball in a bowl [10, 12], and of a roulette like system [11].

The following important properties of doubly transient chaos were pointed out in references [9, 11]:

- Basin boundaries appear to be fractal, but when observed at increasing magnification fractality is diluted out, a feature called slim fractal in reference [11],
- Finite-time Lyapunov exponents characterizing the initial dynamics are positive,

- The survival probability of trajectories away from the attractors decays dramatically in time.

The aim of this paper is to explore additional properties of doubly transient chaos. One important general observation is that a clear view of doubly transient dynamics is provided by identifying the basic phase space structures of the dissipation-free case (KAM tori or chaotic regions) and by following their time evolution with dissipation turned on. The idea of this approach grows out of the recent advancement in the theory of general non-autonomous systems, pointing out the need for an ensemble view.

The concept of the ensemble view was born in dynamical systems theory, where the seminal article [13] drew attention to the fact that in the case of changing parameters a single long trajectory traces out a fuzzy shape, while an ensemble of motions starting from many different initial conditions generates a structured pattern at any instant. In such cases *individual trajectories turn out to be not representative*, while the use of ensembles provides statistically well established results. The ensemble-related pattern, the so-called snapshot chaotic attractor, changes its shape all the time. The concept of snapshot attractors was applied to understand a variety of physical phenomena (see e.g. [14–19]). The concept was rediscovered in a climatic context [20–25], and is widely used since then (see e.g. [26–31]). This ensemble based concept has recently been applied to epidemics [32] and to Hamiltonian systems subjected to time-dependent parameters [33, 34], too.

An important consequence of these studies on driven systems is that an ensemble based view is appropriate for a faithful statistical representation of systems with changing parameters. The distribution of the ensemble members in the phase space defines a measure. This is the analog of the natural measure of traditional chaos theory, but changes in time. Averages are to be taken with respect to this distribution at any instant of time. As a consequence, the ensemble view makes an *instantaneous* characterization of the dynamics possible (there is no need to carry out the usual $t \rightarrow \infty$ limit, which would be most often misleading in systems permanently changing in time).

In contrast to the mentioned examples, doubly transient chaos is without any driving or positive feedback, and hence without any energy injection. As a consequence, the overall energy is strictly decreasing in such cases, and this *internal* parameter change is the analog of the change of the driving amplitude in the cases mentioned above.

One-dimensional undriven systems cannot be chaotic, the simplest systems producing doubly transient chaos are thus two-dimensional with a four-dimensional phase space. Hence, an ensemble in the phase space is difficult to visualize. To pursue an ensemble approach, we choose sub-ensembles to be monitored e.g. in the form of the KAM tori of the dissipation free system. By the expression *sub-ensemble* we emphasize that the set of trajectories we follow is selected specially, not as typical, from a compact region of the phase space. A Poincaré map of such Hamiltonian systems is a faithful planar representation of the dynamics, and the ensembles based on such tori remain for a while quasi two-dimensional, and thus visualizable on a plane after switching on the dissipation. We shall see that the tori often smoothly deform first, but later they become disintegrated and dissolve in a kind of chaos. The choice of tori is motivated by their simple geometrical appearance, but chaotic regions of the Hamiltonian case can also be chosen as sub-ensemble, whose time evolution in the dissipative dynamics is particularly useful in studying the long-term decay of chaos.

Besides illustrating the sub-ensemble based monitoring of the dynamics, we also illustrate that even if the system possesses a single fixed point attractor, such as the double pendulum or the bouncing on the double wedge, a basin structure can be identified. This is achieved by augmenting the dynamics with a kind of symbolic encoding, and distinguishing the attractors carrying different codes. For example, in case of the double pendulum, we can assign a number to any initial condition based on how many times the lower pendulum wheels around before settling to rest due to energy loss. We show that the dilution of fractality can be observed in the basin boundaries of these attractors, too. Furthermore, we introduce new dynamical quantities for the characterization of doubly transient chaos. These are

- Time-dependent pairwise separation averaged over the sub-ensemble, and
- Instantaneous stretching rate, or topological entropy, as a function of time.

Both quantities enable a time-dependent characterization of the dynamics. They increase initially as in any traditional chaos, but later their increase slows down and stops, according to the fact that chaos ceases to exist ultimately.

To illustrate the general concepts, paradigmatic examples of autonomous dissipative systems will be taken: the magnetic pendulum with air drag, the afore-mentioned double pendulum with friction, and bouncing on a double wedge in the presence of a restitution coefficient less than unity.

In the next section we present the equations of motion of these systems, by deriving the dynamics of the dissipative double wedge in the appendix. Next, we turn to the dissipation free (Hamiltonian) limits which are the starting points to our analysis. The basins of attractions of the original dissipative problem are shown in section 4 on a plane of constant energy to make a comparison with the Hamiltonian phase space possible. We also illustrate here that symbolic encodings can be used to visualize the effect of coexisting attractors even if only

a single asymptotic resting state exists. The evolution of sub-ensembles initiated on KAM tori or chaotic regions of the Hamiltonian case is followed in the presence of dissipation in section 5, and illustrates the nontrivial fate of these phase space objects. Section 6 is devoted to a study of the average pairwise separation evaluated over a sub-ensemble. The slope of this quantity can be considered an instantaneous Lyapunov exponent which, after an initial phase, typically decreases and sooner or later becomes negative indicating the end of chaos, and the start of the ultimate decay. Next we turn to the stretching dynamics of line segments. The slope of the arc length vs time provides an instantaneous topological entropy with an analogous time evolution to that of the Lyapunov exponent. Our summary and conclusions are given in section 8.

2. Examples of doubly transient chaos

2.1. Magnetic pendulum

The system consists of three identical magnets at the corners of a regular triangle of unit edge-length in a horizontal plane. The pendulum is formed by an iron bob suspended from above the center of the triangle through a massless rod. The bob is subjected to the influence of gravity, attractive magnetic forces, and drag due to air friction. For simplicity, we further assume that the length of the pendulum rod is long compared to the distance between the magnets, which allows us to describe the dynamics of the bob entirely in terms of the (x, y) -coordinates of a plane in which the bob carries out harmonic oscillations with a natural frequency ω_0 . This plane is parallel to the plane of the magnets a distance d above it. Following references [6, 7, 9], we assume, for simplicity, an inverse-square law interaction between the bob and the magnets as if they were point magnetic charges. The resulting dimensionless equations of motion are

$$\ddot{x} = -\omega_0^2 x - \beta \dot{x} + \sum_{i=1}^3 \frac{x_i - x}{D_i^3}, \quad (1)$$

$$\ddot{y} = -\omega_0^2 y - \beta \dot{y} + \sum_{i=1}^3 \frac{y_i - y}{D_i^3}, \quad (2)$$

where (x_i, y_i) are the coordinates of the i th magnet, β is the damping coefficient resulting from air drag and assumed to be linear, for simplicity, and $D_i = \sqrt{(x_i - x)^2 + (y_i - y)^2 + d^2}$ are the distances from the pendulum bob to the i th magnet. The time unit is chosen so that the dimensionless magnet strengths are unity. The coordinates of the magnets are $(x_1, y_1) = (\frac{1}{\sqrt{3}}, 0)$, $(x_2, y_2) = (-\frac{1}{2\sqrt{3}}, -\frac{1}{2})$, and $(x_3, y_3) = (-\frac{1}{2\sqrt{3}}, \frac{1}{2})$.

In our simulations $\omega_0 = 0.5$ and $d = 0.3$, which is representative of all cases for which the fixed point at the origin is unstable, and β is taken from the interval $(0.01, 0.14)$.

2.2. Double pendulum

The double pendulum consist of a pendulum attached to the end of another pendulum pinned to a fixed support. The angle of the upper pendulum with the vertical is θ_1 , that of the lower pendulum is θ_2 . We assume that the lower and the upper pendulums have the same mass m and length ℓ , and they are both subjected to gravity. The equation of motion of double pendulum is given in several textbooks, see e.g. [35]. Friction is assumed here to be proportional to the angular velocity of the upper pendulum and to the relative angular velocity between the lower and upper pendulums. Measuring the time in units of $\sqrt{\ell/g}$ with g being the gravitational acceleration, the dimensionless equations of motion are

$$\ddot{\theta}_1 = \frac{\sin(\theta_2 - \theta_1)[\dot{\theta}_2^2 + \dot{\theta}_1^2 \cos(\theta_2 - \theta_1) + \cos \theta_2] - \sin \theta_1}{2 - \cos^2(\theta_2 - \theta_1)} - \beta \dot{\theta}_1, \quad (3)$$

$$\ddot{\theta}_2 = -\frac{\dot{\theta}_2^2 \cos(\theta_2 \theta_1) + 2\dot{\theta}_1^2 + 2 \cos \theta_1}{2 - \cos^2(\theta_2 - \theta_1)} \sin(\theta_2 - \theta_1) - \beta(\dot{\theta}_2 - \dot{\theta}_1). \quad (4)$$

Here β characterizes the strength of friction and is taken from the interval $(0.01, 0.1)$.

2.3. Bouncing on a double wedge

Perhaps the simplest example of chaotic behavior in non-driven conservative physical systems leading to a discrete time dynamics is provided by a ball bouncing in vacuum between two slopes of identical inclinations α facing each other [7, 35, 36]. In reality, however, some kind of dissipation is present, and energy conservation does not hold. Here we consider the case when the bounce is not elastic, the normal component, w , of the velocity after the bounce is $k < 1$ times that of the incoming value in modulus, where k is a restitution coefficient. The parallel component, u , does not change. The description of the motion is based solely on the knowledge of oblique projection. It is worth recording the velocity vector right after the instants of the bounces,

and constructing a kind of Poincaré map from this. The positions at the instant of the collisions then follow from the conservation of energy, which is valid in-between the collisions, while the paths between collisions are the well known parabola arcs.

It is worth writing the entire map in a dimensionless form by measuring energy in terms of the initial energy E_0 per unit mass of ball. Velocity (u, w), distance and time are measured in units of $\sqrt{2E_0}$, E_0/g , and $\sqrt{E_0}/(2g^2)$, respectively. The dimensionless dynamics, in which E_n is the energy per unit ball mass, u_n is the velocity component parallel with the slope right after the n th collision, and z_n is the square of the perpendicular component, reads as (see appendix)

$$E_{n+1} = E_n + \frac{k^2 - 1}{k^2} z_{n+1}, \quad (5)$$

Case 1: bouncing on the same slope

$$u_{n+1} = u_n - 2\sqrt{z_n} \tan \alpha, \quad (6)$$

$$z_{n+1} = k^2 z_n. \quad (7)$$

This form applies if

$$(u_n - 2\sqrt{z_n} \tan \alpha)^2 + z_n < E_n. \quad (8)$$

Case 2: bouncing over on the other slope

$$u_{n+1} = -u_n + \sqrt{z_n} \tan \alpha - \frac{\sqrt{z_{n+1}}}{k} \tan \alpha, \quad (9)$$

$$z_{n+1} = k^2 [(u_n \sin 2\alpha + \sqrt{z_n} \cos 2\alpha)^2 + (2E_n - 2u_n^2 - 2z_n) \cos^2 \alpha]. \quad (10)$$

Without energy loss, for $k = 1$, we recover the conservative mapping derived in [7, 35, 36]. The basic difference is that the energy is constant in that case, and the map is two-dimensional. The presence of a nontrivial coefficient of restitution broadens the dynamics with another variable (E_n), hence what we see when following the motion in the (u, z) plane is thus only a projection of the full dynamics. In our simulations we use $\alpha = 50^\circ$ and $k = 0.8$.

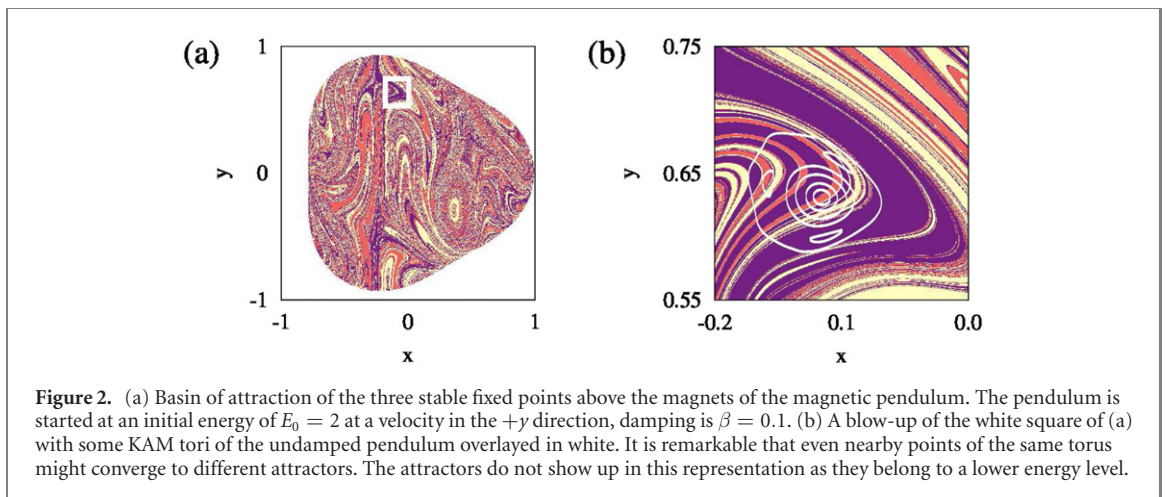
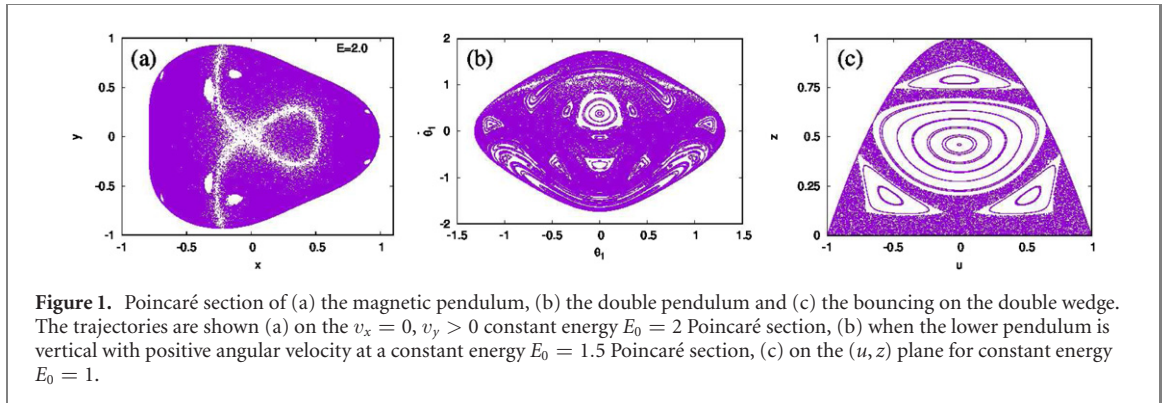
This map, derived in the appendix, is the analogue of monitoring the dynamics of the previous two examples on a Poincaré map (by prescribing e.g. the vanishing of one of the velocity components in the magnetic pendulum, or the vertical position of the lower pendulum in the double pendulum). The full dissipative dynamics is described by a three-dimensional map on such a Poincaré section, while the Hamiltonian limit is two-dimensional on the same section due to the preservation of the energy.

3. The dissipation-free limit

After witnessing the experimental presentation of the motion in any of our paradigmatic examples, one is likely to remember that the presenter's explanation describes the phenomenon of chaos without mentioning dissipation, but when, after perhaps minutes, an overall decay sets in, the presenter says something like 'and now the motion stops, of course, due to the presence of unavoidable dissipation'. Even if the time of a few oscillation/bounces during the observation in such demonstrations is not sufficient to carry out a systematic investigation of chaos properties, the scene sketched suggests that we are intending to consider the motion dissipation-free for short times at least. In addition, the authors of [9] suggested that systems that are chaotic without dissipation are expected to exhibit doubly transient chaos. These observations motivate us to take a closer glance on the Hamiltonian limit of such systems.

When dissipation is neglected, the phase space volume is conserved. In this case, typically the phase space consists of regions with chaotic and regular behavior. This is illustrated in figure 1 for all three systems we investigate.

The knowledge of the Hamiltonian case is not only important because the root of doubly transient chaos might be here, but because the sub-ensembles mentioned in the introduction are worth taking from this phase space. One might of course wish to take a uniform distribution over the full available phase space as an extended ensemble, and follow its deformation in the dissipative dynamics. A more detailed view is obtained, however, if we choose either a torus or a chaotic region. This way we can also follow if, and for how long, these basic components keep their regular or chaotic character in the dissipative dynamics. Before these issues are discussed in section 5, we turn in the next section to the analysis of basin structures, in relation to the Hamiltonian patterns of the phase space.



4. Basin of attraction

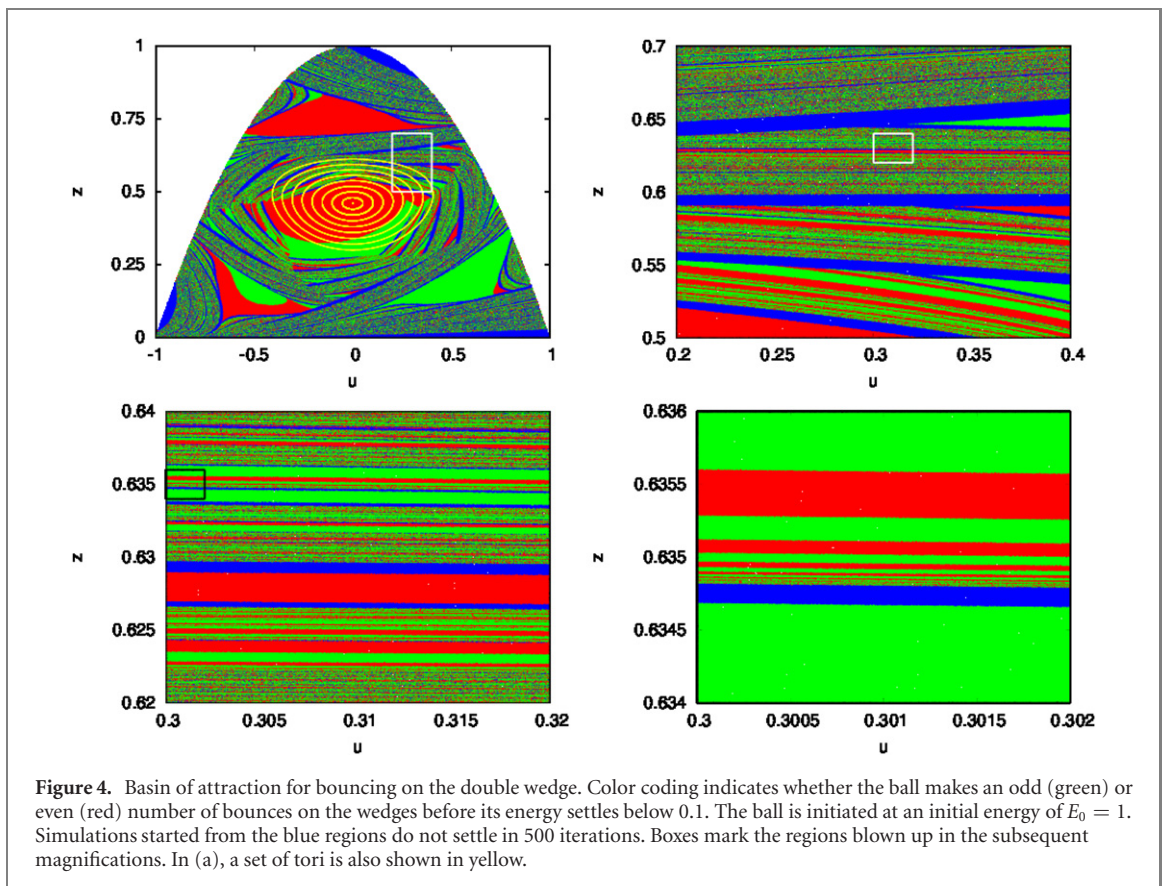
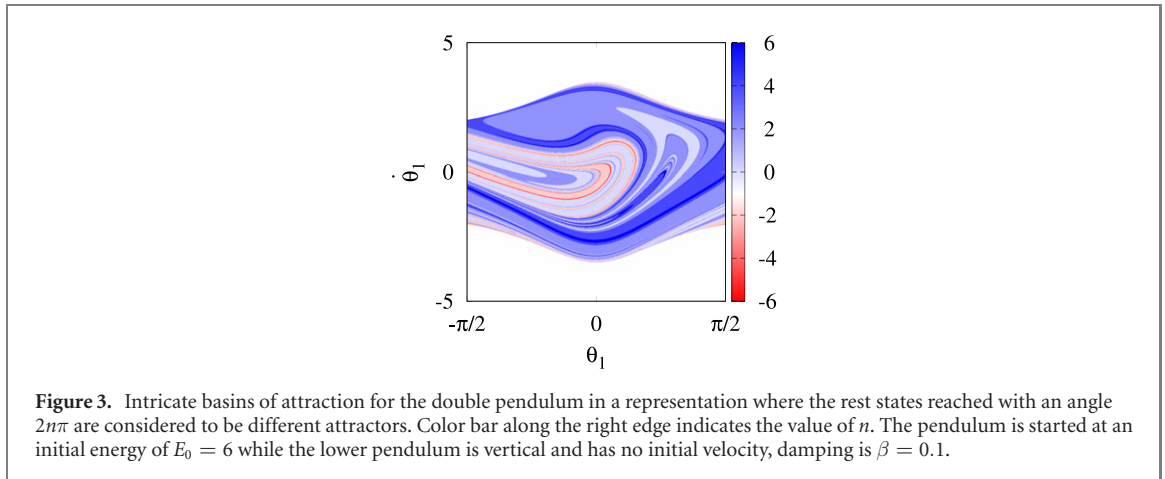
Possibly the most charming characteristics of traditional transient chaos is the pattern of basins of attraction, which typically possesses fractal properties. Phase space regions leading to different outcomes of the dynamics are the consequence of the existence of a chaotic saddle, a set of trajectories never settling to any attractor, whose stable manifold forms the nontrivial boundary between the basins of attraction.

Whether such fractal objects exist in purely damped systems is questionable. These systems cannot possess trajectories that are not settling to a fixed point attractor, with damping all motion ceases after long enough time. However, we still see nontrivial boundaries between phase space regions leading to different attractors, as e.g. in references [6, 7, 9–11, 12].

The characteristic geometry of doubly transient chaos was shown to exhibit the slim fractal property by Chen *et al* [11]. The authors show that most often the boundaries are true fractals in the sense that successive magnifications of the boundaries provide new details at arbitrarily small scales. In other cases, the boundaries form finite-scale fractals which become simple below a finite resolution. Both options fall under the category of slim fractals whose fractal dimension is associated with a given length scale, and, in particular, it decreases with the decrease of this length scale. They also argue that the use of the so-called equivalent dimension enables one to capture the fractal scaling over all scales. Since these generic features were illustrated with an impressive numerical accuracy (in a simplified roulette dynamics) in [11], we provide here only a qualitative study of additional basin-related features.

In the usual representation of basins of attraction, the particles are released from rest, hence the energy is not constant over the configuration space. We choose here the constant energy representation and release particles uniformly distributed according to the condition with which the Poincaré section is defined. This way a direct comparison of the basin structure with the Hamiltonian phase space becomes possible.

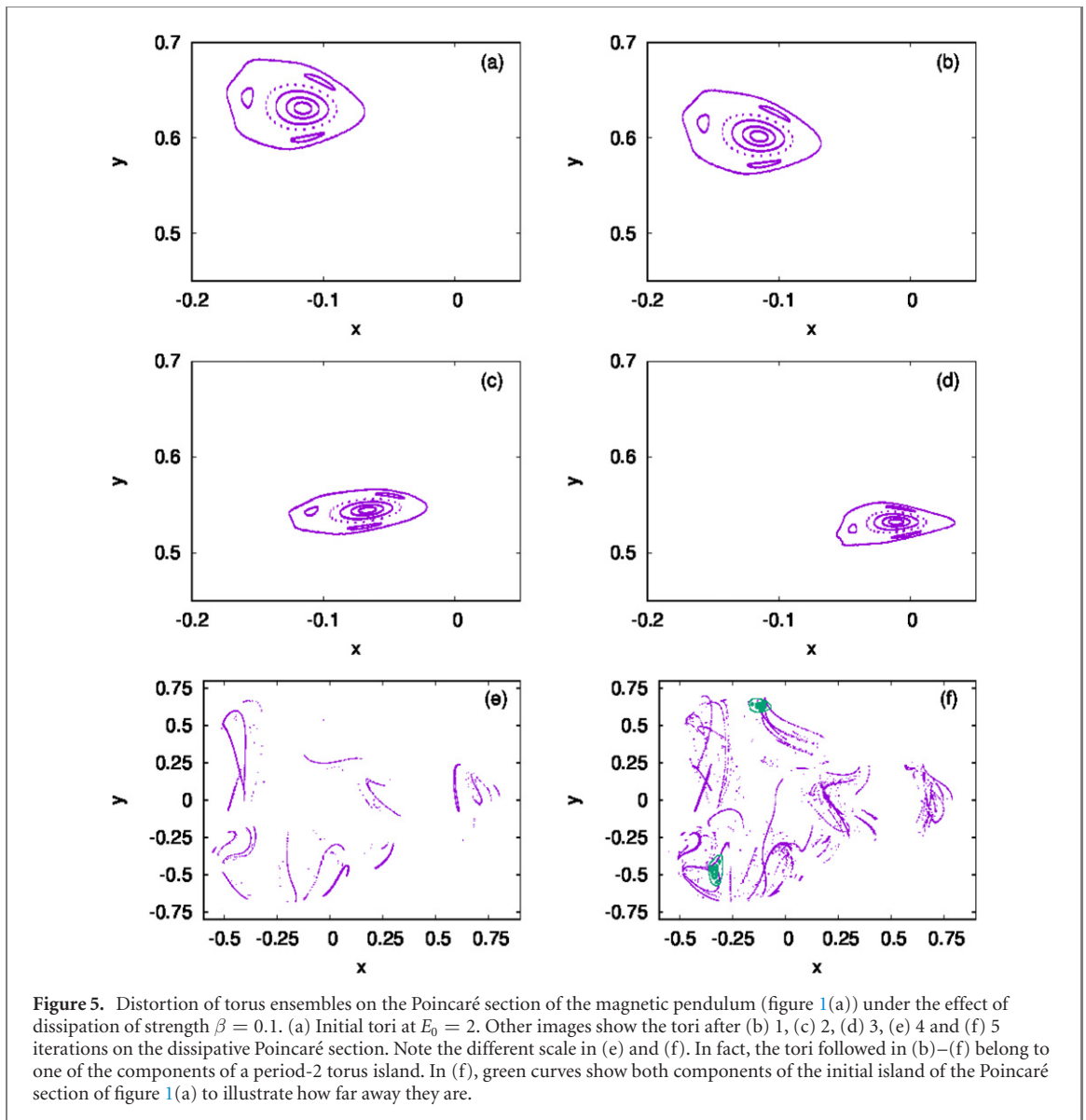
As an example, we show in figure 2 the basin of attraction of the magnetic pendulum. The image shows by color coding which attractor is reached by the pendulum initiated above that point with an initial energy $E_0 = 2.0$ with zero velocity in the x direction. We see that the boundary between the colors shows an intricate structure. Whether this boundary is seemingly fractal or not depends on both the initial energy and the dissipation. For small initial energy or for large dissipation the boundary is a simple curve. For large initial energy



or small dissipation, as in figure 2 for large energy, the trajectories have more time to mix before settling to an attractor, hence the boundary becomes more intricate.

For the double pendulum, there is only one physical end state in the long run: the stable state with both pendulums hanging down. However, we show that it is still possible to plot basin boundaries if the end states with different number of complete turns are considered to be different. In figure 3, color coding shows n as a function of the initial state where the final angle of the lower pendulum is $2n\pi$. Here the initial energy is large, $E_0 = 6$, and the phase space is completely chaotic, see also figure 6(a). We, again, observe (not shown) that the intricate boundary disappears for small initial energy E_0 and large dissipation.

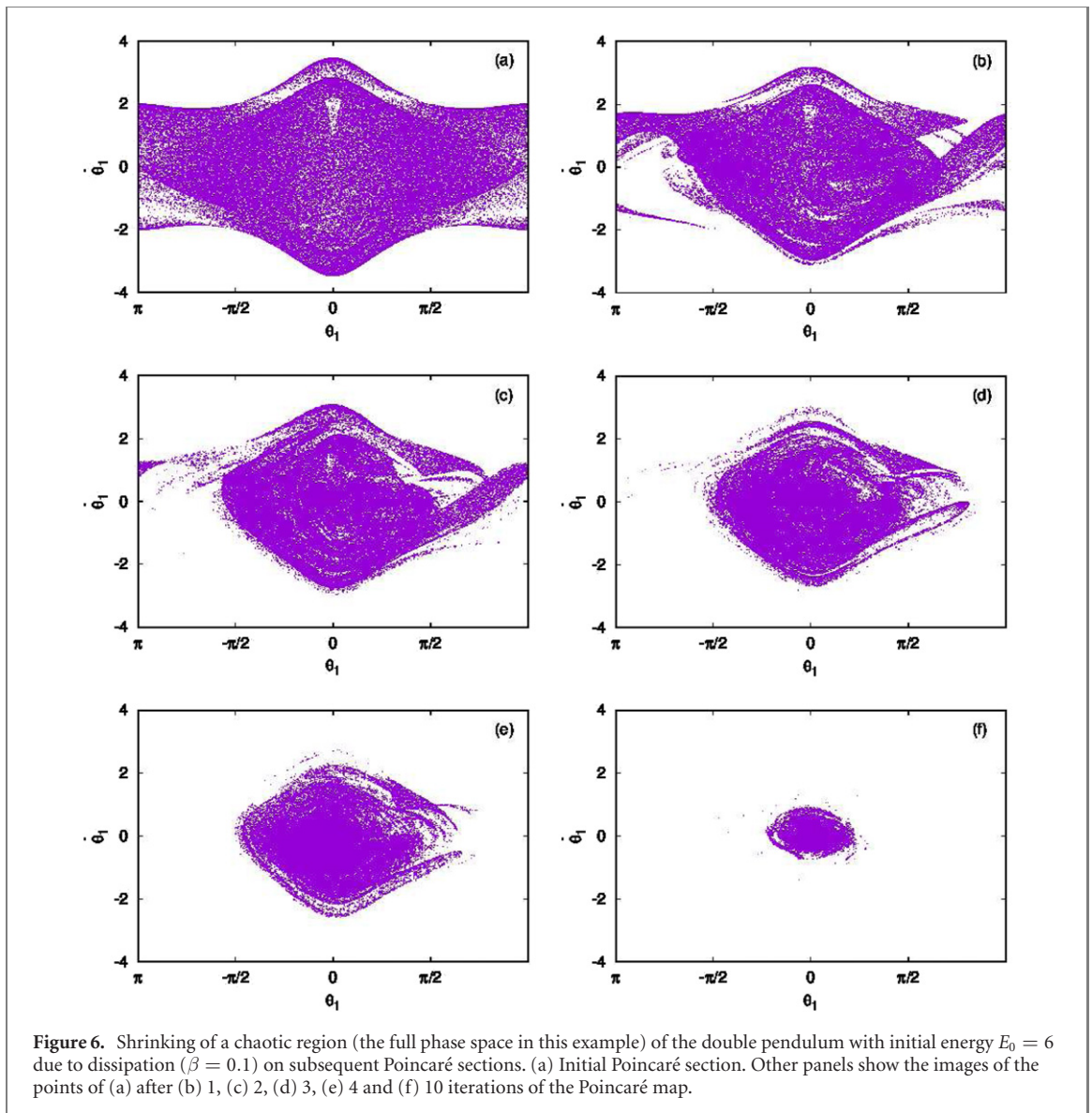
As in case of the double pendulum, bouncing on the double wedge also has only one attractor, the resting state in the origin, in the lowest point of the wedge. However, we can color code the initial states in the (u, z) plane according to whether they make an odd or even number of bounces on either wedge before their energy settles below a threshold. The result is shown in figure 4. Here we also see in the subsequent magnifications that the apparent fractality is diluted.



5. Evolution of phase space objects

To investigate the effects of dissipation, we initialize ensembles on the basic components of the Poincaré sections illustrated in figure 1, with dissipation turned on right after. First, in figure 5 we show how the KAM islands of the magnetic pendulum already shown in figure 2(b) are distorted when dissipation takes effect. We see that the islands slowly distort during the first three Poincaré maps (see figures 5(b)–(d)). Then, they abruptly fall apart into segments, which is likely a consequence of the fact that the images of the tori have become so much extended in the four-dimensional phase space that pieces of them do not cross the plane ($v_x = 0$) of the Poincaré section at the same time as the rest of the ensemble. The last panel (figure 5(f)) suggests that later the segments become convoluted in a large portion of the phase space. We can say that these tori break up as time goes on, and become entrained into a phase space region of strong stretching. Later, in section 6 we shall demonstrate quantitatively that the stretching is exponential, indicating that the ensemble which exhibited initially regular dynamics has evolved to be chaotic. A similar scenario of torus evolution, namely that tori become cut into pieces first, and later they enter a region of strong stretching, was identified recently in a non-dissipative system with time-dependent parameters [34]. In figure 5(f) it is also clear that remnant lines of the tori intersect indicating that the full phase space of the Poincaré section is three-dimensional in the presence of dissipation, and what we see on the (x, y) plane is a projection from 3D.

Although in systems exhibiting doubly transient chaos many tori behave like the ones shown here, there could exist tori which do not break up, just deform and shrink. In particular, tori designating small amplitude oscillations about elliptic points characterizing simple stable states, which become converted into a fixed point attractor of the asymptotic dissipative dynamics, must behave so since in linear systems no chaos can exist.



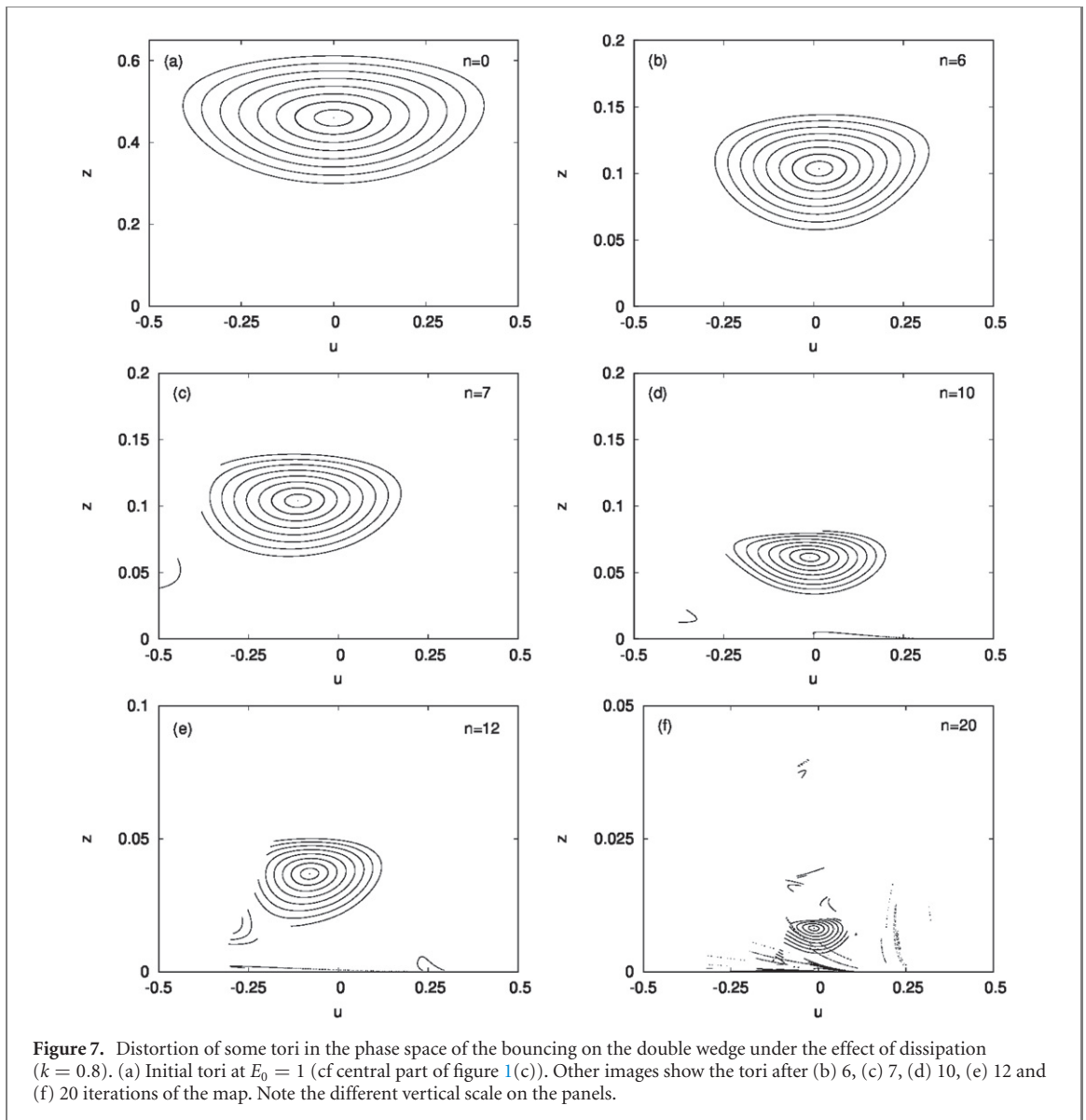
When selected tori do not break up for any reason, one has the option of selecting a chaotic region from the Hamiltonian phase space and following its evolution in the presence of dissipation to characterize doubly transient chaos. In our next example we therefore choose an energy value at which no macroscopic tori exist.

In figure 6, we show what happens to the chaotic region of the double pendulum's phase space at $E_0 = 6$ under the effect of dissipation. As dissipation takes effect, the available phase space becomes smaller due to the decrease in the energy, indicating, at the end, a convergence towards the point of the single attractor of rest at the origin.

In figure 7, we show, again, the distortion of some tori in case of the bouncing on the double wedge. We see that the outermost torus falls apart after the 6th iteration (figure 7(c)). This is the consequence of some trajectories initiated on the outermost torus falling on the wedge opposite to that of the rest of trajectories, hence following a completely different time history. Later, after the 10th iteration, more tori start to break. However, we can still follow clearly the segments of the tori, they do not disintegrate completely. This implies that they are not behaving chaotically yet. However, as we wait a bit longer, we start to see an exponential separation along the remains of the tori, as shown in the next section. Note that a few small tori about the center appear to survive up to the end, illustrating the co-existence of non-broken tori with the broken ones in the long run.

6. Time-dependent Lyapunov exponents

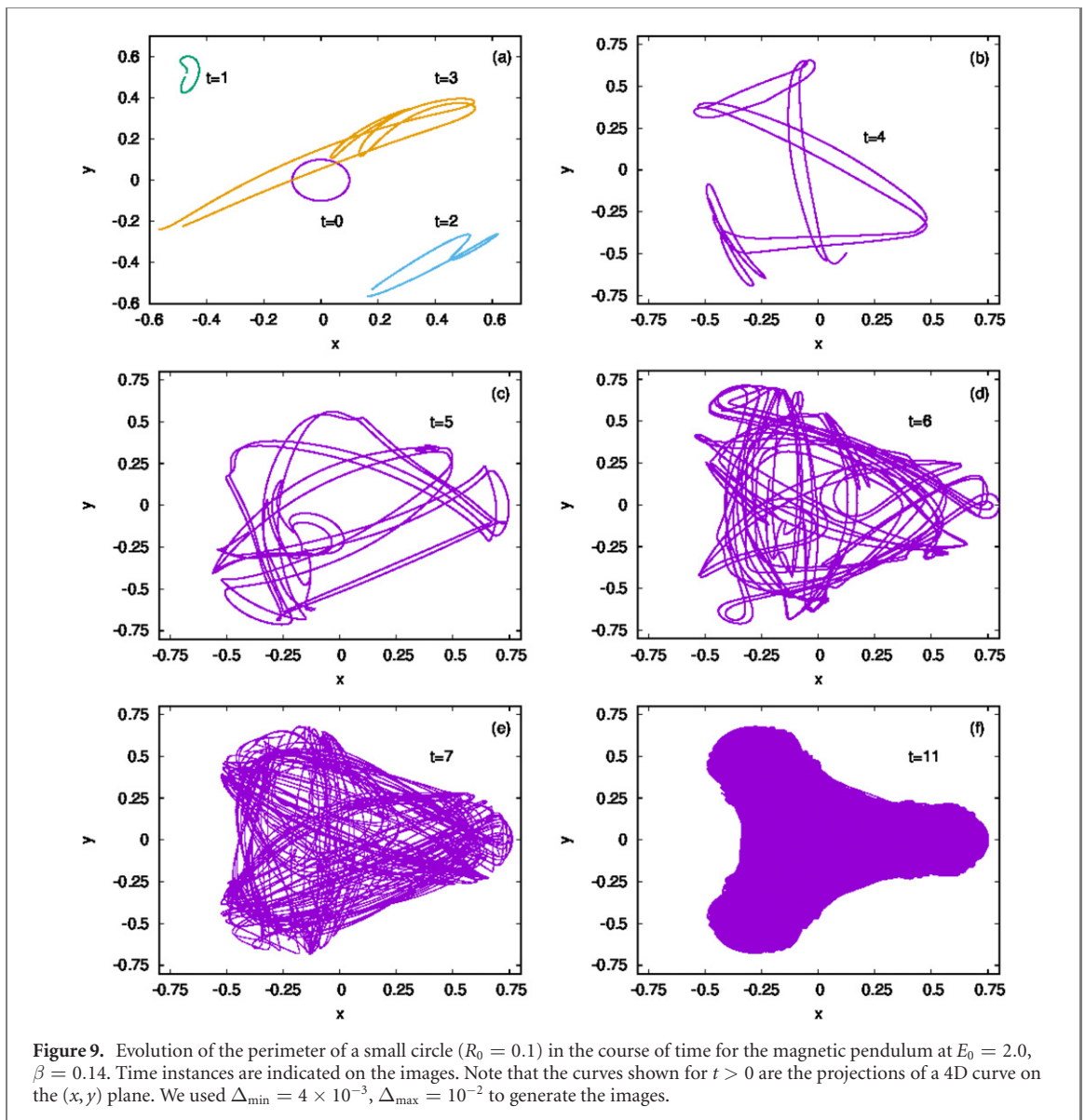
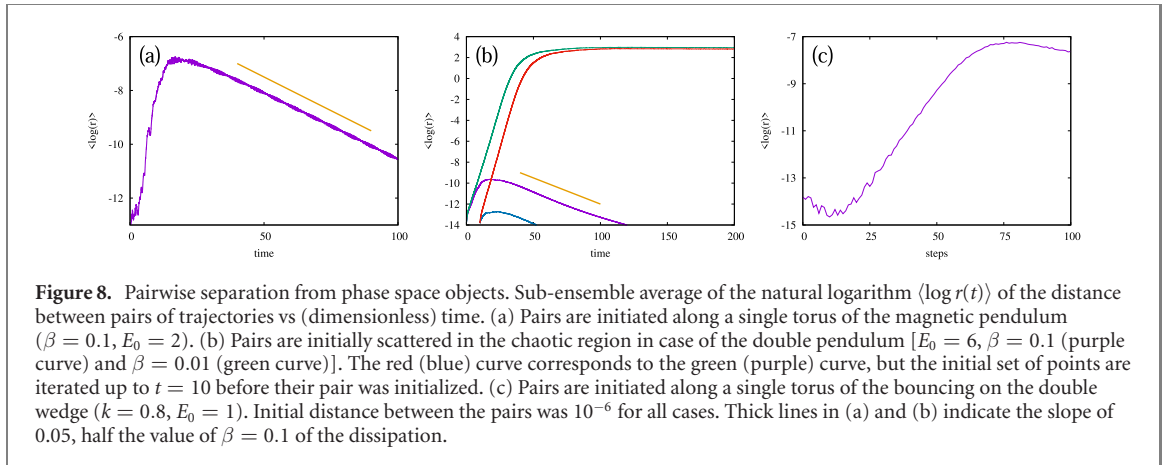
In doubly transient chaos, hardly any standard tool of chaos characterisation can be applied. In particular, the celebrated periodic orbit expansion (see e.g. reference [37]) does not apply in the lack of the existence of



an infinity of hyperbolic cycles. Now we show that a quantitative characterisation of doubly transient chaos is possible via a few, well chosen dynamical quantities which are in analogy with those applied in traditional chaos theory. The quantities treated in this and the next section enable an *instantaneous* characterization of the dynamics which allows the monitoring of weakening and disappearance of chaos features. The mentioned quantities are plotted in continuous time, instead of on Poincaré sections in case of the magnetic and the double pendulum.

In order to compute traditional Lyapunov exponents, we start pairs of initially close trajectories and measure their exponential rate of separation in time [4] after averaging over several pairs. In order to see the effect of the dissipation on the basic components of the phase space, we apply a Lyapunov exponent-like quantity suggested recently to characterize time-dependent systems [33, 34]. We restrict the computation of the separation between trajectories to pairs initiated in a *sub-ensemble* and the average is taken over this sub-ensemble which is either a KAM torus or a chaotic region.

For the magnetic pendulum we take a large number of trajectories on one of the tori at a fixed initial energy E_0 and initiate a couple to each of these trajectories with slightly different initial conditions. Then we follow their dissipative dynamics and measure the ensemble averaged logarithm of the pairwise distance $\langle \log r(t) \rangle$ over the torus where $r(t)$ is the distance between the pairs of initially close trajectories at time t . The slope of this curve can be considered the *instantaneous Lyapunov exponent* of the dynamics. As long as the initial torus remains in a non-chaotic region, $\langle \log r(t) \rangle$ does not change too rapidly. However, when we experience the disintegration of a torus after some time, this quantity starts to grow exponentially as shown in figure 8(a). This initial slope corresponds to the finite time Lyapunov exponent investigated in [9]. Before a saturation is reached, that is, the average distance becomes comparable to the size of the available phase space at that



energy, the growth rate of this logarithmic quantity starts to decrease. This indicates that the strength of chaos, the time-dependent Lyapunov exponent, is becoming smaller and smaller. At the maximum of $\langle \log r(t) \rangle$, no average growth is present, the Lyapunov exponent vanishes at this instant. We have to conclude that chaos ceases here.

After this, the average distance decreases: this is a consequence of the shrinking of the available phase space whose volume changes proportionally to $\exp(-2\beta t)$ due to dissipation. The thick line segment in figure 8(a) has a slope of 0.05, half of the dissipation rate β . On average, we expect that the long-time behavior about the fixed points is governed by a coordinate and velocity decay proportional to $\exp(-\beta t/2)$ as in the case of damped oscillators, energy decays thus with β . Since the linear extension of the available phase space decays with the square root of the energy, which limits the actual distance between the pairs of points, we expect a slope in figure 8(a) to be $\beta/2$.

Similarly, in figure 8(b) we show the ensemble average of $\log r(t)$ in a chaotic region of the double pendulum. In this case, the pairs are chosen from the chaotic region which fills the full phase space visible in figure 6(a). We can see that there is an exponential separation right from the beginning. After a maximum is reached with strong dissipation, the average distance starts to decrease with the size of the available phase space, the thick line above the lower curve shows the slope 0.05, half of the dissipation rate. This decaying part of the curve indicates the lack of chaos, and the start of the stopping of any motion. In this panel two graphs are shown, one (purple) for a strong and one (green) for a weak dissipation. This second case illustrates that chaotic-like behavior can indeed be observed over several periods if friction is weak, as is the case in many actual experimental demonstrations. Even if so, this is not permanent chaos, rather a stretched doubly transient chaotic behavior.

In figure 8(b), we also show the time evolution of $\langle \log r(t) \rangle$ when first 1000 points are iterated from the chaotic region according to the dissipative dynamics for a period of $t = 10$ before their pairs were initiated at a distance 10^{-6} beside them. We see that for small dissipation ($\beta = 0.01$), $\langle \log r(t) \rangle$ does not change much. This is quite reasonable, as the size of the phase space is almost the same during this period, we sample the same chaotic behavior. However, when the dissipation is large ($\beta = 0.1$), the size of the available phase space shrinks considerably by the time $t = 10$ when the pairs are initialized. Chaos is much weaker by this instant, hence we see a smaller initial slope and a much smaller distance that can be reached by the pairs, the maximum of $\langle \log r(t) \rangle$ is smaller but the slope of the decay remains 0.05.

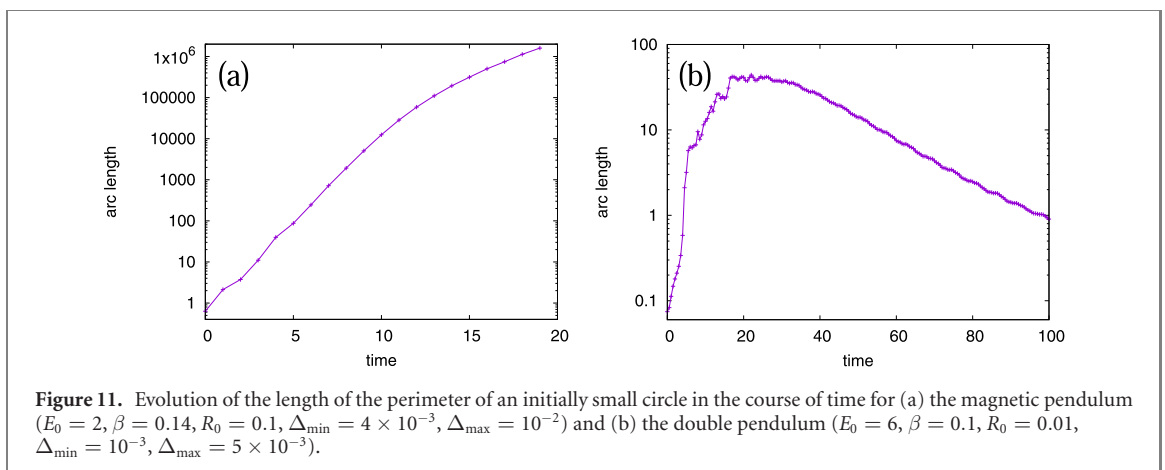
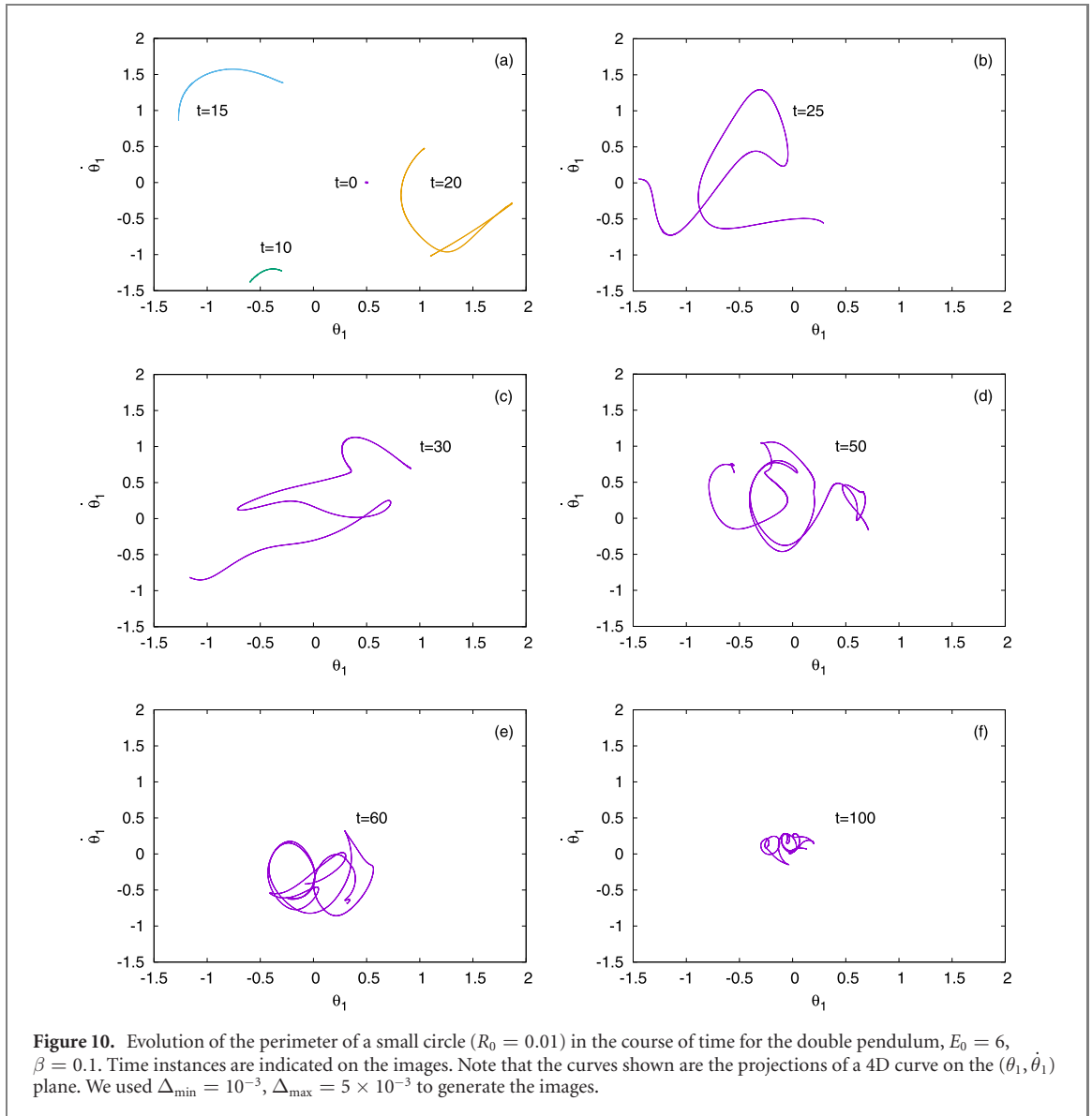
Figure 8(c) shows the same for a single torus of the bouncing on the double wedge. We see an initial shrinking here due to dissipation, then after around 15 iterations an exponential growth starts. This is the instant when the torus breaks and dissolves in a chaotic region. After saturation, the average distance, again, decays with the size of the available phase space.

7. Stretching and folding

A ubiquitous phenomenon in chaotic systems is the stretching and folding of a continuous ensemble of trajectories in phase space. This is illustrated in figure 9 for the magnetic pendulum and in figure 10 for the double pendulum. In these figures, an initially small circle of initial conditions is followed in time. Initially, 120 points were selected on a circle of radius R_0 , and their evolution in time is simulated. If two neighboring points get further from each other in phase space than a predefined small value of Δ_{\max} , new points are inserted between them so that distances between neighboring points become smaller than this value. Similarly, if the distance between neighboring points becomes smaller than Δ_{\min} , one of the points is omitted. This algorithm is restricted to time continuous systems, hence maps, and thus the double wedge problem, are not treated in this section. A similar but general concept, the expansion entropy (a quantity depending on the time instant when a long-term observation starts), has been developed [38], but for doubly transient chaos our approach seems to be more adaptable.

We see in figure 10 for the double pendulum that after some time the actual length starts to decrease with the shrinking of the available phase space due to energy loss.

In figure 11 we show the time evolution of the arc length for both cases. The growth rate of this quantity is known to be proportional to the topological entropy [38, 39] in traditional cases. This chaos measure characterizes the topological complexity of the dynamics, and its positivity is a sign of transient chaos [4]. We see that this positivity is fulfilled in the first part of both graphs, although the rate, the *instantaneous topological entropy*, is not constant. For the magnetic pendulum, figure 9 suggests a monotonous increase up to $t = 11$, but figure 11(a) also reveals that the rate starts to deviate from the initial one at about this instant, and the deviation continuous up to the end of the simulation at $t = 20$. The fact that the maximum is reached in figure 11(b) at about the 20th iterate for the double pendulum, is consistent with the maximum reached in the purple curve of figure 8(b), indicating that chaos ceases to exist in the double pendulum with a strong dissipation quite early.



8. Summary and conclusions

This paper sheds new light on doubly transient chaos by also focusing on the dissipation-free limit. Our investigations reinforce the statement of reference [9], namely that the *origin of doubly transient chaos is the permanent*

chaos of the Hamiltonian limit. As a consequence, one does not expect the appearance of doubly transient chaos in any system with an integrable dissipation-free limit.

We have pointed out that an interesting insight can be obtained into the dynamics by presenting basin boundaries (perhaps with attractors symbolically encoded) at fixed energies. Furthermore, monitoring either KAM tori or chaotic regions of the Hamiltonian case on Poincaré maps of the dissipative dynamics provides a detailed view on how chaos spreads or shrinks. The fact that tori can break up and dissolve in chaos shows that in the first phase of doubly transient chaos regular motion might become converted into chaos. In a sense, all elements of the phase space converge to the snapshot attractor determined by the structures of the Hamiltonian phase space. The long-term character of this attractor is certainly nonchaotic.

We have offered here two quantities which are able to follow in time how the strength of chaos changes in the system: a finite time Lyapunov exponent like and a topological entropy like measure. They both typically grow initially, and as long as they are positive, we consider the dynamics chaotic, but after reaching a maximum, they start to decay. The time instant of the maximum designates the time when chaos ceases in the system.

In summary, let us list the characteristics of doubly transient chaos explored in [9, 11] and here. In such systems

- Basin boundaries (even with symbolically encoded attractors) appear to be fractal at first sight, but with increasing resolution fractality is diluted out, that is, the basin boundaries become smooth for high enough resolution in the investigated cases,
- The survival probability away from the attractors decays dramatically in time,
- Time-dependent ensemble averaged finite-time Lyapunov exponents are positive first but turn to be negative after some time,
- Topological entropy (or instantaneous stretching rate) is positive first and starts decreasing later on.

Doubly transient chaos appears to be the only possible form of chaos in undriven dissipative systems. There is thus a plethora of cases in which this phenomenon occurs. A notable example might be coin tossing or dice throwing in which a complex basin structure was found but the literature considers the dynamics just non-chaotic [40–43], not yet doubly transiently chaotic. A general feature of all these cases is that when such systems become periodically driven, they exhibit traditional chaotic dynamics as exemplified for the magnetic pendulum in reference [9] and also for the double pendulum in reference [44].

A dynamical view behind the listed features is the existence of a time-dependent chaotic set, a snapshot chaotic saddle, outside the fixed point attractor(s) which changes in time, and after a weakening period the set loses its chaotic character and supports an ultimate stopping dynamics. Such a transient chaotic saddle governing the initial decay was constructed in [9] for the magnetic pendulum, but similar objects are expected to exist in all doubly transient cases. In an even more general context, any system subjected to parameter drift, even if driven or non-dissipative or without a final state of rest, can only exhibit transients, as no stationarity is present and chaos characteristics change in time. They thus can also be regarded to be examples of generalized doubly transient chaos [45]. In this spirit, even chaotic advection in decaying open fluid flows has recently been considered as an example of doubly transient chaos [46].

Acknowledgments

We thank Adilson Motter for calling our attention to the phenomenon today called doubly transient chaos, and for several interesting discussions during writing [9] and afterwards. We would like to thank Dániel Jánosi for beneficial discussions and comments. This work was supported by the Hungarian NKFIH Office under Grant Nos. K-125171 and K 128584, and by the NRD Fund TKP2020 IES under Grant BME-IKA-VIZ.

Data availability statement

The data that support the findings of this study are available upon request from the authors.

Appendix. Derivation of the dissipative double wedge dynamics

A.1. The map

Let us denote the total energy per unit mass, and the tangential and normal velocity components right after the n th bounce by E_n , and u_n and w_n , respectively. After the bounce, the energy is

$$E_n = \frac{u_n^2 + w_n^2}{2} + gy_n, \quad (11)$$

where y_n is the height coordinate of the bounce on the slope. Positioning the origin of the reference frame into the break point between the two slopes, the x coordinate is obtained as $x_n = y_n \tan \alpha$ as long as the bounce takes place on the right slope, and it is $x_n = -y_n \tan \alpha$ on the left slope.

The energy is conserved up to the instant preceding the next bounce. In this instant the velocity components are u_{n+1} , w_{n+1}/k , and y_{n+1} . Therefore

$$\frac{u_{n+1}^2 + (w_{n+1}/k)^2}{2} + gy_{n+1} = E_n, \quad (12)$$

holds. After the bounce,

$$E_{n+1} = \frac{u_{n+1}^2 + w_{n+1}^2}{2} + gy_{n+1}. \quad (13)$$

From these it follows that

$$E_{n+1} = E_n + \frac{k^2 - 1}{2k^2} w_{n+1}^2, \quad (14)$$

that is the map for the energy is very simple and depends only on w_{n+1} .

The u, w dynamics basically differs depending on whether the next bounce is on the same slope or not. In both cases it is worth choosing our coordinate system so that the ξ axis is parallel to the surface of the slope on which the next bounce occurs, while axis η is normal to it and points upwards, the origin of the (ξ, η) system is the same as that of the (x, y) system. This implies that the ξ and η components of the gravitational acceleration are, respectively, $g \sin \alpha$ pointing towards the origin along the ξ axis and $g \cos \alpha$ pointing opposite of direction η .

Case 1. If the ball does not jump to the other slope, both bounces take place along the ξ axis. The initial distance of bounce n from the origin is $y_n/\sin \alpha$. The initial velocities are

$$v_{\xi,0} = u_n, \quad v_{\eta,0} = w_n. \quad (15)$$

The time t_n elapsed until the next bounce follows from the η displacement

$$\eta = w_n t - \frac{g \cos \alpha}{2} t^2 \quad (16)$$

being zero. Thus

$$t_n = \frac{2w_n}{g \cos \alpha}. \quad (17)$$

The velocity components evolve in time after bounce n as

$$v_\xi = u_n - g \sin \alpha t, \quad \text{and} \quad v_\eta = w_n - g \cos \alpha t. \quad (18)$$

The parallel and normal velocity components before bounce $n+1$ are $\tilde{u}_{n+1} = v_\xi(t_n)$ and $\tilde{w}_{n+1} = -v_\eta(t_n)$. The velocities after the bounce are $u_{n+1} = \tilde{u}_{n+1}$, $w_{n+1} = -k\tilde{w}_{n+1}$. Thus

$$u_{n+1} = u_n - 2w_n \tan \alpha, \quad w_{n+1} = kw_n. \quad (19)$$

This is the Poincaré map of bouncing on a single slope. It describes that the parallel velocity increases in modulus, while the normal one decreases due to the dissipation.

This case applies if y_{n+1} is positive, i.e., if according to (12)

$$\frac{u_{n+1}^2 + (w_{n+1}/k)^2}{2} < E_n = E_{n+1} - \frac{k^2 - 1}{2k^2} w_{n+1}^2. \quad (20)$$

From this

$$u_{n+1}^2 + w_n^2 < 2E_n, \quad (21)$$

or

$$u_{n+1}^2 + w_{n+1}^2 < 2E_{n+1}. \quad (22)$$

In terms of the original velocities the former implies

$$(u_n - 2w_n \tan \alpha)^2 + w_n^2 < 2E_n. \quad (23)$$

Case 2. Without the restriction of generality, we assume that bounce n is on the right slope, while the next one takes place on the left one. The ξ axis is thus parallel to the plane of the left slope. Since the origin of the reference frame is the break point between the two slopes, the right slope has an inclination angle 2α to

the ξ axis. The point of the n th bounce is of distance $y_n/\sin \alpha$ from the origin, the initial η coordinate is thus $y_n/\sin \alpha \times \sin 2\alpha = y_n 2 \cos \alpha$.

The initial velocities after bounce n in the ξ and η directions are now

$$v_{\xi,0} = -u_n \cos 2\alpha + w_n \sin 2\alpha, \quad v_{\eta,0} = u_n \sin 2\alpha + w_n \cos 2\alpha. \quad (24)$$

The time t_n elapsed until the next bounce follows again from the η coordinate

$$\eta = y_n 2 \cos \alpha + v_{\eta,0} t - \frac{g \cos \alpha}{2} t^2, \quad (25)$$

being zero. The positive solution of this quadratic equation is

$$t_n = \frac{v_{\eta,0} + D_n}{g \cos \alpha}, \quad (26)$$

where

$$D_n = \sqrt{v_{\eta,0}^2 + 4gy_n \cos^2 \alpha}, \quad (27)$$

is the discriminant. The velocity components evolve in time after bounce n as

$$v_\xi = v_{\xi,0} - g \sin \alpha t, \quad \text{and} \quad v_\eta = v_{\eta,0} - g \cos \alpha t, \quad (28)$$

and the parallel and normal velocity components before bounce $n+1$ are $\tilde{u}_{n+1} = v_\xi(t_n)$ (u is positive if it points away from the origin) and $\tilde{w}_{n+1} = v_\eta(t_n)$. The velocities after the bounce are $u_{n+1} = \tilde{u}_{n+1}$, $w_{n+1} = -k\tilde{w}_{n+1}$. This leads to

$$u_{n+1} = v_{\xi,0} - v_{\eta,0} \tan \alpha - D_n \tan \alpha. \quad (29)$$

After substituting the initial velocities (24)

$$u_{n+1} = -u_n + w_n \tan \alpha - D_n \tan \alpha. \quad (30)$$

Similarly,

$$w_{n+1} = -k(v_{\eta,0} - v_{\eta,0} - D_n) = kD_n. \quad (31)$$

To make the mapping closed in u, w, E , we express in D_n the velocities in terms of u_n, w_n , and y_n in terms of E_n , and obtain

$$w_{n+1}^2 = k^2 [v_{\eta,0}^2 + (4E_n - 2u_n^2 - 2w_n^2) \cos^2 \alpha], \quad (32)$$

$$= k^2 [(u_n \sin 2\alpha + w_n \cos 2\alpha)^2 + (4E_n - 2u_n^2 - 2w_n^2) \cos^2 \alpha],$$

$$w_{n+1}^2 = k^2 [u_n^2 (\sin^2 2\alpha - 2 \cos^2 \alpha) + w_n^2 (\cos^2 2\alpha - 2 \cos^2 \alpha) + u_n w_n \sin 4\alpha + 4E_n \cos^2 \alpha]. \quad (33)$$

A.2. Billiard with the new variable z

It is worth introducing the new variable $z \equiv w^2$ proportional to the kinetic energy carried by the velocity component perpendicular to the slope. Thus, the full three-variable (E, u, z) map reads as

$$E_{n+1} = E_n + \frac{k^2 - 1}{2k^2} z_{n+1},$$

Case 1.

$$u_{n+1} = u_n - 2\sqrt{z_n} \tan \alpha,$$

$$z_{n+1} = k^2 z_n.$$

The advantage of using z is that this map has a constant Jacobian $J = k^2$.

Case 1 applies if

$$(u_n - 2\sqrt{z_n} \tan \alpha)^2 + z_n < 2E_n.$$

Case 2.

$$u_{n+1} = -u_n + \sqrt{z_n} \tan \alpha - \frac{\sqrt{z_{n+1}}}{k} \tan \alpha,$$

$$z_{n+1} = k^2 [(u_n \sin 2\alpha + \sqrt{z_n} \cos 2\alpha)^2 + (4E_n - 2u_n^2 - 2z_n) \cos^2 \alpha].$$

A.3. Dimensionless form

It is worth writing the entire map in a dimensionless form by measuring energy in terms of the initial energy E_0 . Velocity (u, w), distance and time are measured in units of $\sqrt{2E_0}$, E_0/g , and $\sqrt{E_0/(2g^2)}$, respectively. The dimensionless dynamics is given in section 2.3.

ORCID iDs

György Károlyi  <https://orcid.org/0000-0002-1021-9554>

Tamás Tél  <https://orcid.org/0000-0003-0983-0804>

References

- [1] Ott E 1981 *Rev. Mod. Phys.* **53** 655
- [2] Grassberger P and Procaccia I 1983 *Physica D* **9** 189
- [3] Katok A and Hasselblatt B 1995 *Introduction to the Modern Theory of Dynamical Systems* (Cambridge: Cambridge University Press)
- [4] Ott E 2002 *Chaos in Dynamical Systems* 2nd edn (Cambridge: Cambridge University Press)
- [5] Mihailescu E 2012 *J. Math. Anal. Appl.* **394** 517
- [6] Peitgen H-O, Jürgens H and Saupe D 2004 *Chaos and Fractals: New Frontiers of Science* (Berlin: Springer)
- [7] Tél T and Gruiz M 2006 *Chaotic Dynamics: an Introduction Based on Classical Mechanics* (Cambridge: Cambridge University Press)
- [8] Lai Y-C and Tél T 2011 *Transient Chaos: Complex Dynamics on Finite-Time Scales* (Berlin: Springer)
- [9] Motter A E, Gruiz M, Károlyi G and Tél T 2013 *Phys. Rev. Lett.* **111** 194101
- [10] Nagy P and Tasnádi P 2016 Irregular chaos in a bowl *Key Competences in Physics Teaching and Learning Proc. of GIREP EPEC 2015* ed E Dębowska and T Greczyło (Wrocław: Institute of Experimental Physics) pp 262–9
- [11] Chen X, Nishikawa T and Motter A E 2017 *Phys. Rev. X* **7** 021040
- [12] Nagy P and Tasnádi P 2018 Double Transient Chaotic Behaviour of a Rolling Ball *Open Access Journal of Physics* **2** 11–6 <https://www.sryahwpublications.com/open-access-journal-of-physics/volume-2-issue-2/3.php>
- [13] Romeiras F J, Grebogi C and Ott E 1990 *Phys. Rev. A* **41** 784
- [14] Yu L, Ott E and Chen Q 1990 *Phys. Rev. Lett.* **65** 2935
- [15] Lai Y-C, Feudel U and Grebogi C 1996 *Phys. Rev. E* **54** 6070
- [16] Lai Y-C 1999 *Phys. Rev. E* **60** 1558
- [17] Serquina R, Lai Y-C and Chen Q 2008 *Phys. Rev. E* **77** 026208
- [18] Ku W L, Girvan M and Ott E 2015 *Chaos* **25** 123122
- [19] Vincze M, Borgia I D and Harlander U 2017 *Sci. Rep.* **7** 254
- [20] Ghil M, Chekroun M D and Simonnet E 2008 *Physica D* **237** 2111
- [21] Ghil M 2019 *Earth Space Sci.* **6** 1007
- [22] Drótos G, Bódai T and Tél T 2015 *J. Clim.* **28** 3275
- [23] Pierini S, Ghil M and Chekroun M D 2016 *J. Clim.* **29** 4185
- [24] Ghil M and Lucarini V 2020 *Rev. Mod. Phys.* **92** 035002
- [25] Tél T, Bódai T, Drótos G, Haszpra T, Herein M, Kaszás B and Vincze M 2020 *J. Stat. Phys.* **179** 1496
- [26] Haszpra T and Herein M 2019 *Sci. Rep.* **9** 3896
- [27] Kaszás B, Haszpra T and Herein M 2019 *Chaos* **29** 113102
- [28] Deser C 2020 *Earth's Future* **8** e2020EF110854
- [29] Haszpra T, Herein M and Bódai T 2020 *Earth Syst. Dyn.* **11** 267
- [30] Bódai T, Drótos G, Herein M, Lunkeit F and Lucarini V 2020 *J. Clim.* **33** 2163
- [31] Haszpra T, Topál D and Herein M 2020 *J. Clim.* **33** 3107
- [32] Kovács T 2020 *J. R. Soc. Interface* **17** 20200648
- [33] Jánosi D and Tél T 2019 *Chaos* **29** 121105
- [34] Jánosi D and Tél T 2021 *Chaos* **31** 033142
- [35] Korsch H J and Jodl H J 1999 *Chaos, a Program Collection for the PC* 2nd edn (Berlin: Springer)
- [36] Lehtihet H E and Miller B N 1986 *Physica D* **21** 93
- [37] Cvitanovic P, Artuso R, Mainieri R, Tanner T and Vattay G 2020 *Chaos: Classical and Quantum* edn 17 (Copenhagen: Niels Bohr Institute) www.ChaosBook.org
- [38] Hunt B R and Ott E 2015 *Chaos* **25** 097618
- [39] Newhouse S and Pignataro T 1993 *J. Stat. Phys.* **72** 1331
- [40] Strzałko J, Grabski J, Perlikowski P, Stefanski A and Kapitaniak T 2009 *Dynamics of Gambling: Origins of Randomness in Mechanical Systems (Lect. Notes Phys. vol 792)* (Berlin: Springer)
- [41] Strzałko J, Grabski J, Stefanski A and Kapitaniak T 2010 *Int. J. Bifurcation Chaos* **20** 1175
- [42] Strzałko J, Grabski J, Stefanski A, Perlikowski P and Kapitaniak T 2010 *Math. Intel.* **32** 54
- [43] Kapitaniak M, Strzałko J, Grabski J and Kapitaniak T 2012 *Chaos* **22** 047504
- [44] Dudkowski D, Wojewoda J, Czołczyński K and Kapitaniak T 2020 *Nonlinear Dyn.* **102** 759
- [45] Jánosi D, Károlyi G and Tél T 2020 Climate change in mechanical systems, preprint
- [46] Vilela R D 2020 Doubly transient chaos in a decaying open flow, preprint, this volume